Effect of Thermal Processing on the Microstructure of Ti-26Al-11Nb: Applications to Fusion Welding

M.J. CIESLAK, T.J. HEADLEY, and W.A. BAESLACK III

The possible microstructures resulting from both fusion and solid-state processing of Ti-26Al-11Nb at. pct (Ti-15Al-21Nb wt pct) have been determined. The particular microstructure produced was primarily a function of the cooling rate from the β solvus. The most rapid cooling rate, associated with pulsed Nd:YAG (yttrium-aluminum-garnet) laser welding, resulted in a microstructure in which the high-temperature β underwent an ordering reaction on cooling to the CsCl (B2) crystal structure. Intermediate cooling rate ($\approx$60 °C/s) specimens [characteristic of the fusion zone and heat-affected zone (HAZ) in arc welds] were found to undergo a complete transformation (no retained β observed) to an acicular α_2 microstructure. Electron microprobe and analytical electron microscopy (AEM) analyses revealed no statistically significant compositional differences spatially within this structure. These two observations suggest that the transformation reaction in this cooling rate regime involves, at least in part, a compositionally invariant shear component. Controlled slow cooling rate (0.1 °C/s) experiments produced Widmanstätten microstructures which were two-phase (α_2 + β). The retained β phase was observed to be highly enriched ($\approx$35 wt pct) in Nb. The transformed α_2 exhibited a very low dislocation density. Solidification cracking of fusion welds was not observed.

I. INTRODUCTION

ADVANCED titantium-aluminum intermetallic alloys have certain properties which make them potentially attractive as aerospace materials.[1] Successful joining of these materials will increase their utility in engineering applications. Virtually all commercial joining operations (welding, brazing, diffusion bonding, *etc.*) involve a high-temperature thermal excursion where properties meticulously imparted by prior thermomechanical processing may be lost. In particular, fusion welding operations necessarily destroy all remnants of prior processing, at least in the fusion zone. Cooling of these welded parts to room temperature often results in the evolution of a microstructure in both the fusion zone and HAZ which bears little resemblance to the preprocessed microstructure. Nonequilibrium transformations are common in steels and conventional Ti alloys.[2-6] Very little work has appeared in the open literature which deals with either joining[7,8] or continuously cooled, transformed microstructures[9,10] in highly alloyed Ti aluminides. No comprehensive study has been reported which examined the effect of cooling rate on the microstructure developed in these Ti aluminides.

The primary purpose of this work was to develop an understanding of microstructural evolution during solidification and subsequent solid-state phase transformation in Ti-26Al-11Nb with the intent of anticipating the response of this material to fusion weld processing. The conclusions drawn, though, are quite general and can be applied to a wide variety of industrial operations involving continuous cooling processing, from rapid water quenching to extremely slow furnace cooling.

M.J. CIESLAK, Senior Member of Technical Staff, Process Metallurgy Division 1833, and T.J. HEADLEY, Senior Member of Technical Staff, Electron Optics Division 1822, are with Sandia National Laboratories, Albuquerque, NM 87185. W.A. BAESLACK III, Professor, is with the Department of Welding Engineering, The Ohio State University, Columbus, OH 43210.

Manuscript submitted July 24, 1989.

II. EXPERIMENTAL PROCEDURE

The heat of Ti-26Al-11Nb used in this study has the composition given in Table I. The material, in the form of 1.7-mm sheet stock, was processed to give a two-phase microstructure of matrix α_2 (ordered hexagonal, $D0_{19}$) with β (bcc) at the α_2 grain boundaries and triple points. Figure 1 shows the as-received microstructure of this alloy. Figures 2(a) and (b) are a backscattered electron image and X-ray map (Nb L_α radiation) pair for the as-received material showing the segregation of Nb to the β phase. Figure 3 is a transmission electron micrograph of the as-received structure showing a typical region which includes both grain boundary β and matrix α_2.

Thermal processing of this material involved two types of experiments. The first set of experiments involved continuously cooling samples from the single-phase β region through the transformation temperature range at various rates. These experiments employed a Gleeble 1500[11] computer-controlled thermal simulation device. This device resistance heats laboratory-scale specimens with pulsed (120 Hz) alternating current. A Pt/Pt-13Rh thermocouple percussion welded onto the midpoint of the specimen provides the feedback signal for control of the thermal cycle. Specimens were 75 mm × 8 mm × 1.7 mm in size and were mounted in water-cooled copper jaws such that a 10-mm separation between the jaws was held during testing. All samples were heated at the rate of 100 °C to 1200 °C/s and held there for 90 seconds. It had been observed previously[7] that this isothermal anneal would produce a β grain size similar to that observed in the HAZ of the gas-tungsten-arc (GTA) welds. Cooling rates of 60 °C and 0.1 °C/s were run. The 60 °C/s cooling rate was the most rapid achievable

Table I. Ti-26Al-11Nb Composition

Element	Wt Pct	At. Pct
Al	14.80	26.0
Nb	21.30	10.8
Fe	0.065	0.05
O	0.058	0.20
N	0.006	0.02
Ti	bal.	bal.

with the equipment and specimen available and was obtained by shutting off the heating current at the end of the 90-second anneal and allowing a free cool to ambient temperature. The 0.1 °C/s experiments were terminated at a temperature of 850 °C and allowed to free cool to room temperature. All tests were conducted in vacuum (2 to 5 $\times 10^{-5}$ torr).

The second set of experiments involved fusion welding, both GTA welding and pulsed Nd:YAG laser welding. All welds were made in an argon atmosphere welding chamber and showed no evidence of surface oxidation. Welding parameters are given in Table II.

To assess the susceptibility of this alloy to fusion zone hot cracking during rapid solidification laser welding, an experiment was performed in which two sheets were butt welded (full penetration, parameters listed above) along the length of a joint (≈50 mm) which was shimmed at both ends to a 0.8-mm opening. The sample was restrained from bending out of plane during welding. Stereomicroscopic and metallographic examinations were performed on the sample subsequent to welding to determine if cracking had occurred.

Analysis of microstructure began with conventional metallography (Kroll's reagent). Electron probe microanalysis (EPMA) was performed on samples ground flat with 1-μm diamond paste. Samples were analyzed in a Cameca MBX microprobe at a beam current of ≈22 nA and an accelerating potential of 15 kV. These conditions resulted in a spatial resolution of ≈1 μm. Profiling was done in 1-μm steps. X-ray maps were also collected. K_α

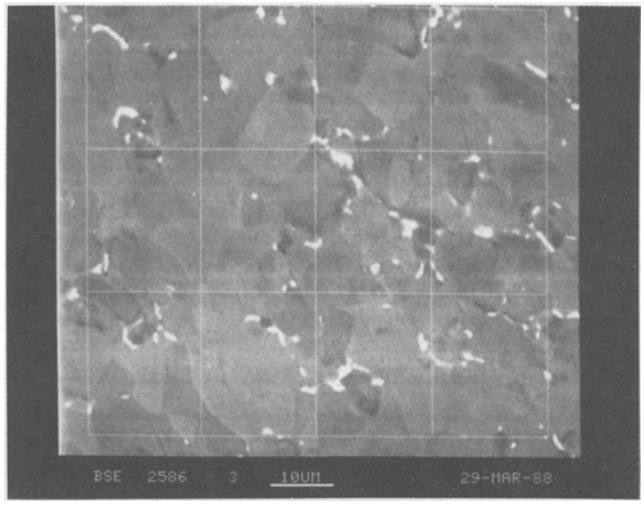

(*a*)

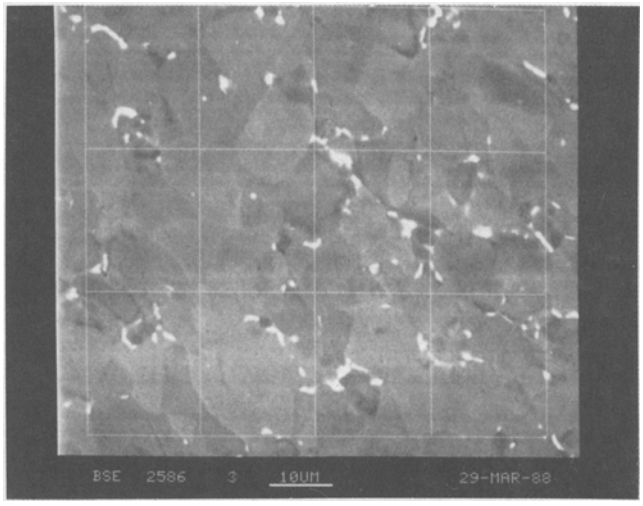

(*b*)

Fig. 2—(*a*) Backscattered electron image and (*b*) Nb L_α X-ray map of as-received Ti-26Al-11Nb.

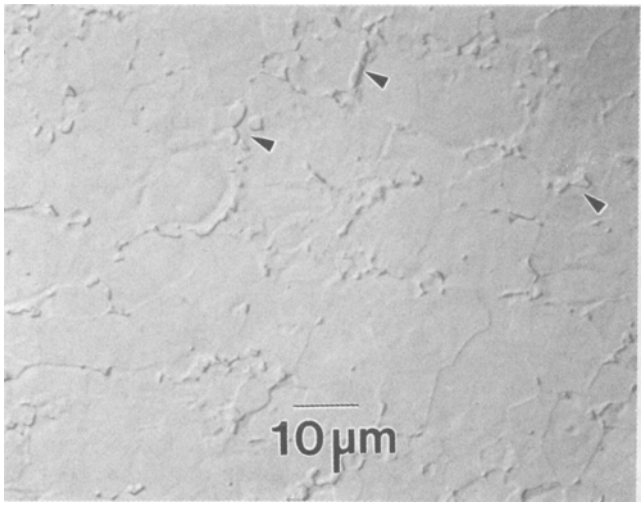

Fig. 1—Optical micrograph of as-received Ti-26Al-11Nb. Arrows indicate positions of β.

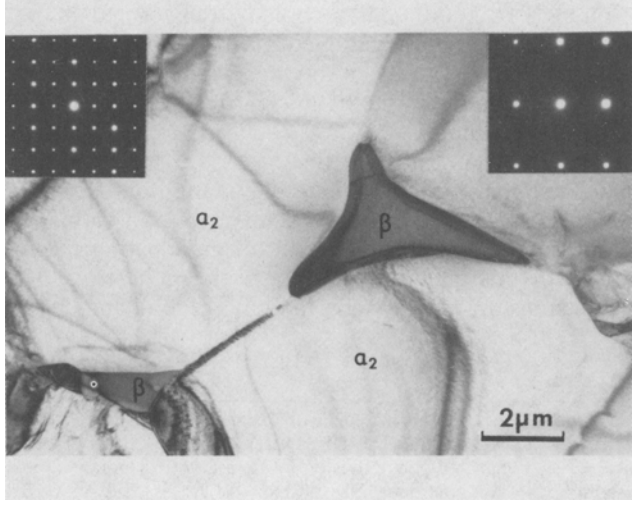

Fig. 3—TEM micrograph of as-received Ti-26Al-11Nb. Diffraction pattern inserts show the [11$\bar{2}$0] α_2 zone (left) and [110] β zone (right).

Table II. Welding Parameters

GTA Welding
90 amps (direct current, electrode negative)
10.5 volts arc voltage
4.2 mm/s travel speed
Pulsed Nd:YAG Laser Welding*
10 Hz
20 J/pulse (200 watts average power)
7.2 ms pulse length
3.8 mm/s travel speed (≈80 pct overlap)
102 mm focusing lens at sharp focus

*Raytheon SS-501-7, 400 watt pulsed Nd-YAG laser welder

characteristic radiation was used for analysis of Ti and Al, with L_α radiation being used for analysis of Nb. Quantitation of EPMA data was performed on a TN5402 utilizing Sandia TASK8.[12]

Analytical electron microscopy was performed on a JEOL 2000FX analytical electron microscope operated at 200 kV and equipped with a TRACOR NORTHERN*

*TRACOR NORTHERN is a trademark of Tracor Northern, Inc., Middleton, WI.

energy dispersive spectroscopy detector/spectrometer for microchemical analysis. Where quantitation was required, background-corrected integrated intensity data were reduced to atomic and weight fractions with a Cliff-Lorimer data reduction routine. Absorption corrections were made for foil thicknesses in excess of 200 nm. Selected-area electron diffraction was used to identify the phases observed. Samples were prepared by jet electropolishing 100-μm-thick disks in a solution of 5 pct sulfuric acid in methanol at −50 °C.

III. RESULTS

A. *Solid-State Continuously Cooled Structures*

1. *60 °C/s cooling rate from 1200 °C*

The Gleeble test samples reveal the microstructures obtained during solid-state processing of this alloy. Figure 4 shows the microstructure obtained from the 60 °C/s cooling rate experiment sample. The structure is characterized by relatively fine acicular features having a transverse dimension of <1 μm. An occasional, barely distinguishable (by optical metallography), constituent is also observed at certain grain boundaries.

An EPMA profile ≈500 μm long along the path indicted in Figure 5(a) is shown in Figure 5(b). Within the resolving capability of the microprobe (≈1 μm), no spatial compositional differences in Ti, Al, or Nb could be identified.

Figure 6 is a transmission electron microscopy (TEM) thin foil micrograph showing the microstructure of this sample on a much finer scale than Figure 4. Several features are of interest. The acicular structure observed in the optical micrograph (Figure 4) is now seen in greater detail. In addition to acicular laths extending over a distance of several microns, much smaller laths are also observed. Selected-area electron diffraction analysis performed on these lath structures revealed that only α_2 (DO_{19}

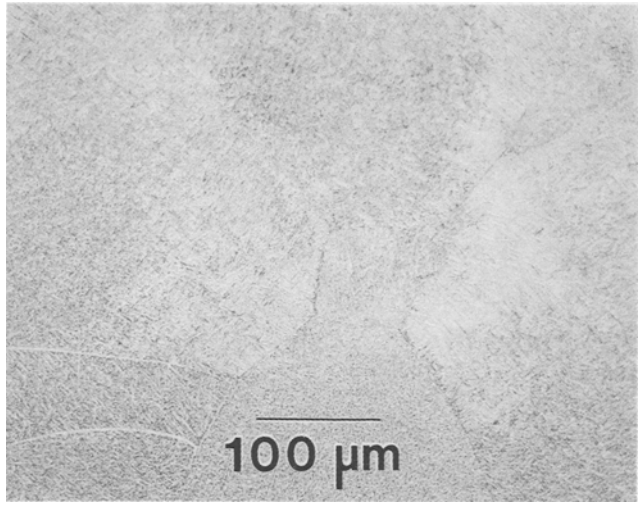

Fig. 4—Optical micrograph of Gleeble processed (60 °C/s) Ti-26Al-11Nb.

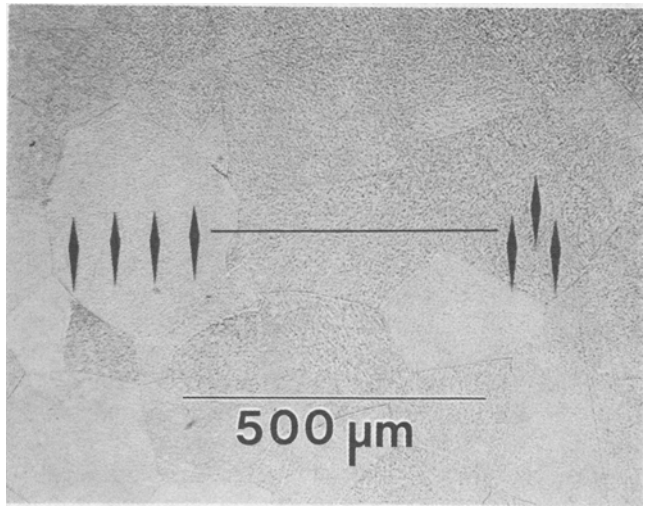

(*a*)

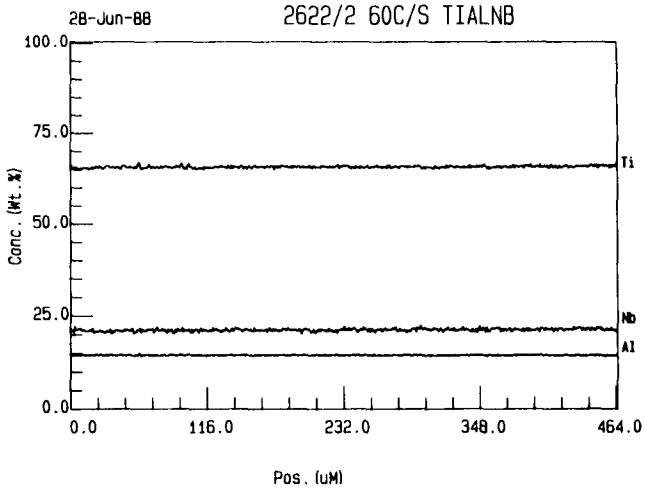

(*b*)

Fig. 5—(*a*) Optical micrograph showing position of microprobe profile in 60 °C/s Gleeble specimen and (*b*) microprobe profile.

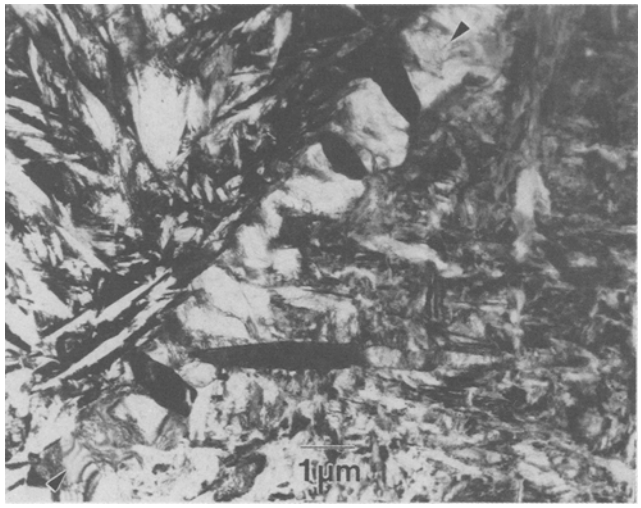

Fig. 6—TEM micrograph of 60 °C/s Gleeble specimen. Arrows indicate position of grain boundary.

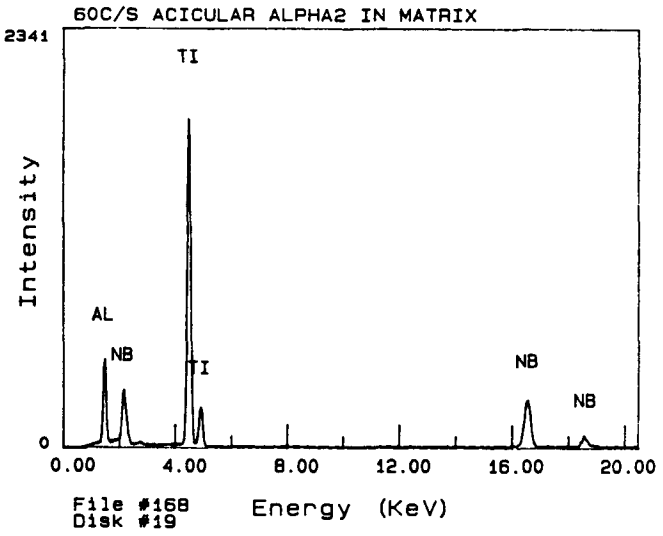

(*a*)

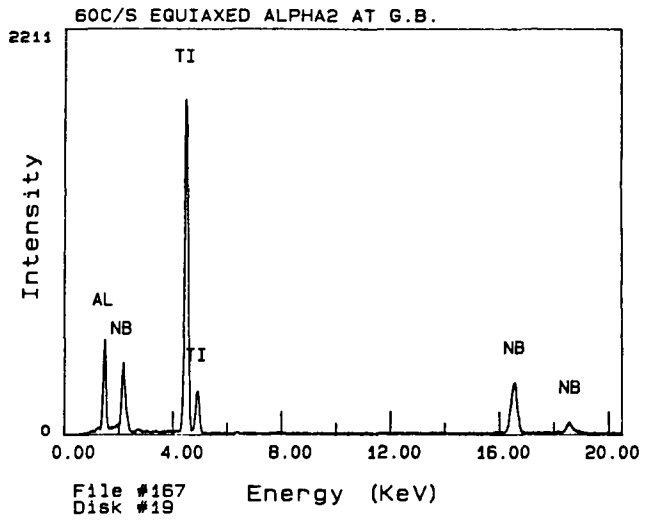

(*b*)

Fig. 7—AEM/EDS spectra obtained from (*a*) acicular α_2 and (*b*) equiaxed grain boundary α_2 in the 60 °C/s Gleeble specimen.

structure) was present. Beta phase was not detected anywhere in this microstructure. A second feature of interest is the higher dislocation density observed in these acicular laths, in contrast to the extremely low dislocation density in the as-received material (Figure 3). The third feature of interest is the structure at the prior β grain boundaries. Selected-area electron diffraction also identified this equiaxed structure as α_2. No β was detected in the equiaxed α_2 area during the diffraction analysis. Energy dispersive spectroscopy analysis performed in the analytical electron microscope revealed no compositional variations anywhere within the acicular structures. Furthermore, within the resolving power of the AEM/EDS analysis, there was no difference in composition between the α_2 laths and the grain boundary α_2. Figures 7(a) and (b) show representative AEM/EDS spectra from the two structures.

Figure 8 shows the cooling curve obtained during the Gleeble processing of the 60 °C/s sample. A thermal arrest is observed (Figure 8(b)) to initiate at ≈893 °C with subsequent recalescence to ≈909 °C. This transformation occurs in approximately 1 second. The smooth cooling curve (Figure 8(a)) subsequent to the transformation indicates that no further reaction occurs involving the liberation of latent heat.

2. *0.1 °C/s cooling rate from 1200 °C*

The Widmanstätten-type microstructure observed in the Gleeble sample processed at a cooling rate of 0.1 °C/s is shown in Figure 9. An EPMA profile made on this sample along the path indicated in Figure 10(a) is shown in Figure 10(b) and reveals extensive partitioning of the three alloying elements between the two phases. Titanium and aluminum segregate together, being enriched in the matrix and depleted in the minor constituent. Niobium is enriched in the minor constituent and depleted in the matrix.

Figure 11 is a TEM micrograph showing the microstructure of the 0.1 °C/s cooled sample. Selected-area electron diffraction confirmed that the matrix phase was α_2 while the minor constituent was β. Analytical electron microscopy/energy dispersive spectroscopy spectra taken from these two phases are shown in Figures 12(a) and (b) and reveal that the β phase is enriched in Nb and depleted in Ti and Al relative to the α_2. Also of interest in Figure 11 is the low dislocation density in both the α_2 and β phases that contrasts with the denser dislocation network observed within the α_2 laths in the 60 °C/s sample.

B. *Weld Structures*

1. *GTA welds*

On a coarse microstructural scale, the fusion zone of the GTA welds is characterized by the presence of a cellular solidification substructure, as shown in Figure 13(a). An EPMA profile taken across these cells is shown in Figures 13(b) and (c). The profile begins in the fusion zone and extends across the fusion line into the HAZ. A periodic modulation of the alloying element distribution is observed in the fusion zone corresponding to

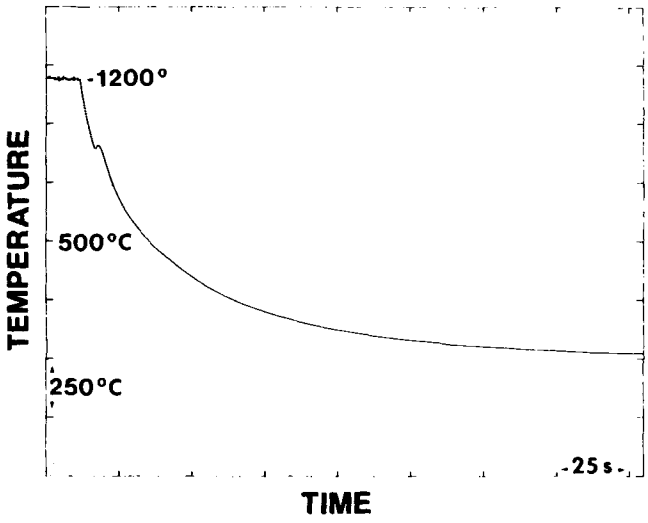

(*a*)

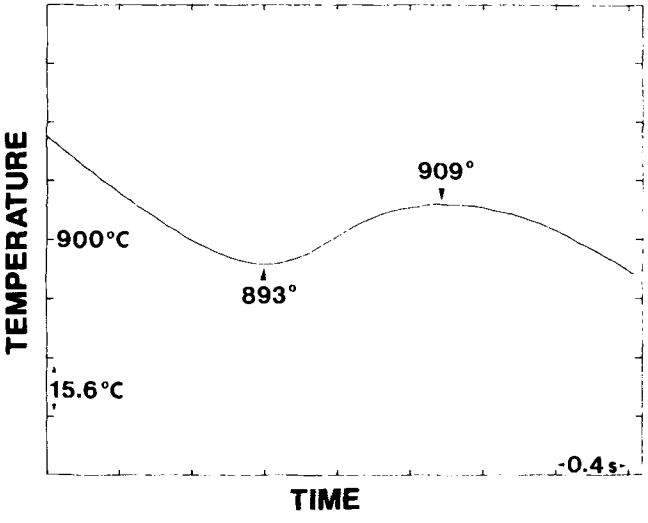

(*b*)

Fig. 8—(*a*) Cooling curve from 60 °C/s Gleeble sample. (*b*) Magnified portion of (a) showing transformation temperature range in greater detail.

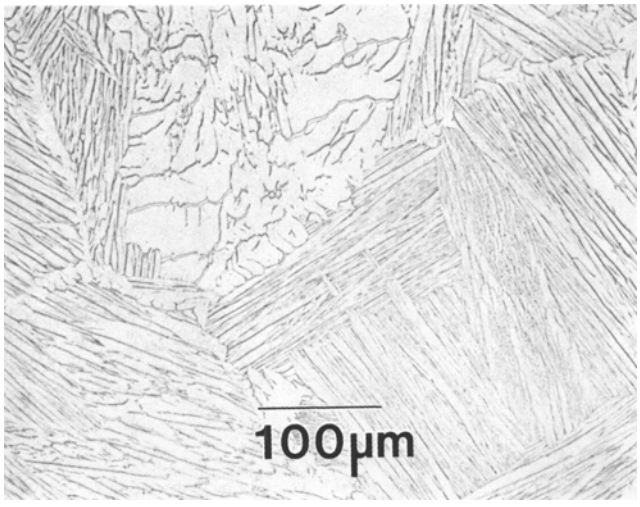

Fig. 9—Optical micrograph of Gleeble processed (0.1 °C/s) Ti-26Al-11Nb.

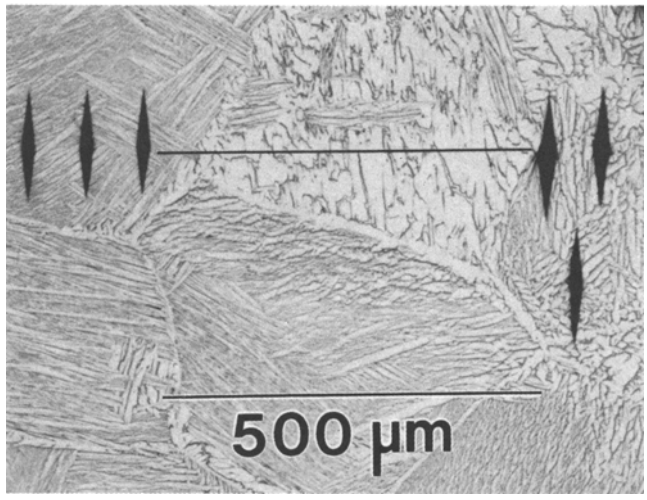

(*a*)

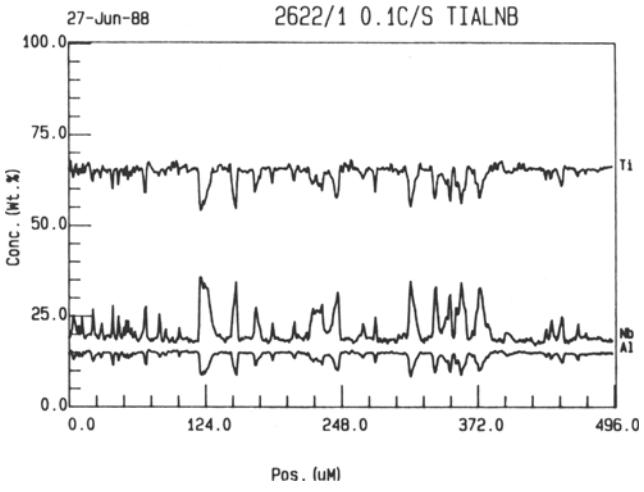

(*b*)

Fig. 10—(*a*) Optical micrograph showing position of microprobe profile in 0.1 °C/s Gleeble specimen and (*b*) compositional profile.

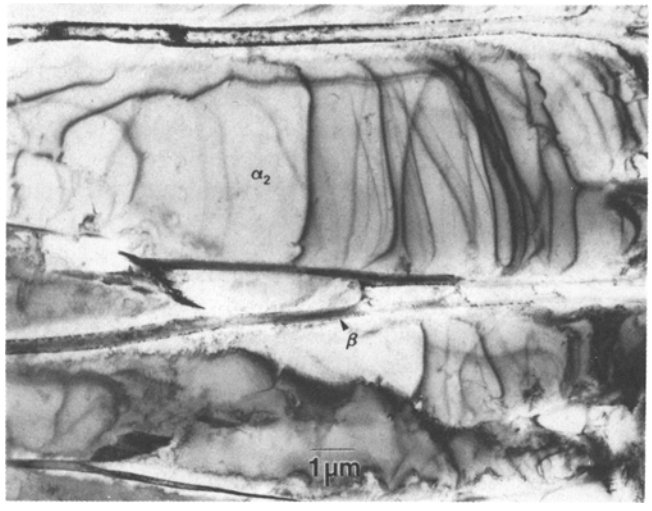

Fig. 11—TEM micrograph of 0.1 °C/s Gleeble specimen.

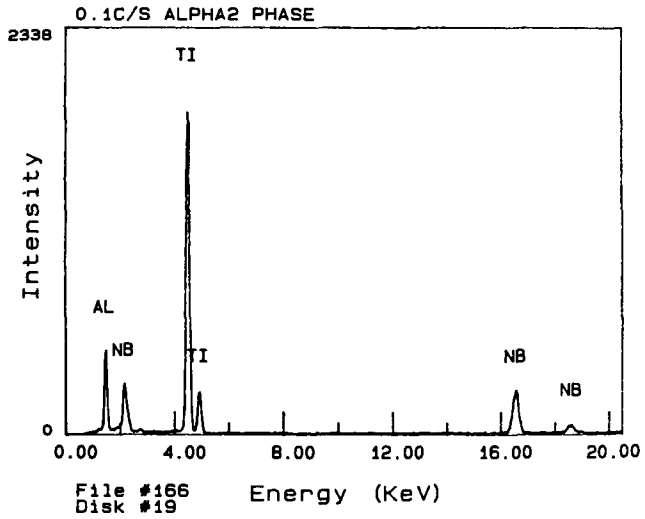

(*a*)

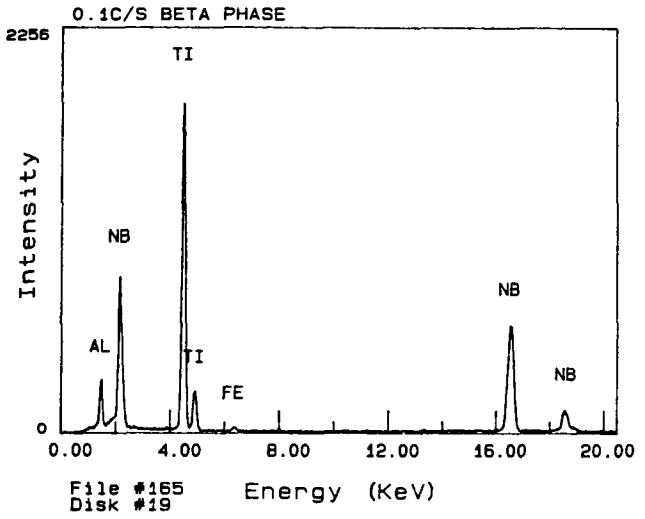

(*b*)

Fig. 12—AEM/EDS spectra obtained from (*a*) α_2 and (*b*) β found in 0.1 °C/s Gleeble specimen.

the cellular solidification pattern. In general, though, the GTA weld fusion zone and HAZ microstructures were similar to that of the 60 °C/s continuously cooled Gleeble sample. An optical micrograph of the fine-scale fusion zone microstructure observed in GTA weld metal is shown in Figure 14. The intragranular morphology is acicular, with an occasional appearance of a distinguishable grain boundary constituent. Figure 15 shows the fusion line region, with the acicular microstructure being continuous across the fusion line.

Figure 16 is a TEM micrograph of the acicular structure found in the fusion zone of the GTA weld. As in the case of the 60 °C/s continuously cooled sample, a grain boundary constituent was also observed. Selected-area electron diffraction analysis revealed that both structures were α_2. Again, no retained β was observed.

A composition profile made in the analytical electron microscope across an acicular α_2 lath in the GTA weld

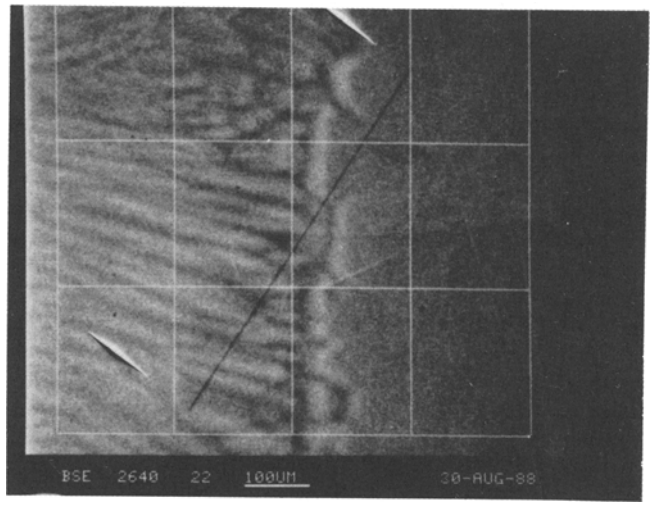

(*a*)

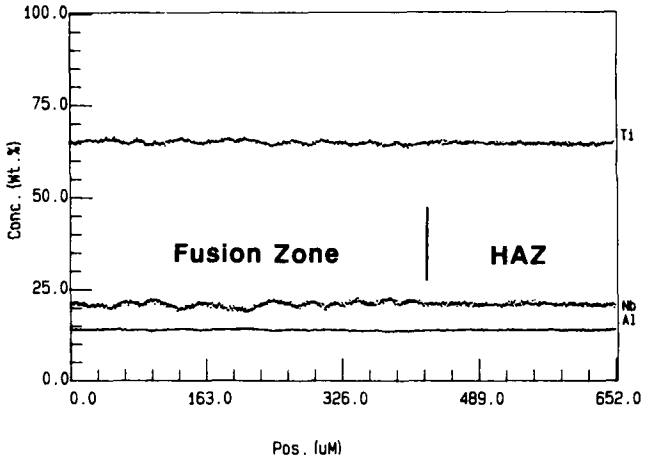

(*b*)

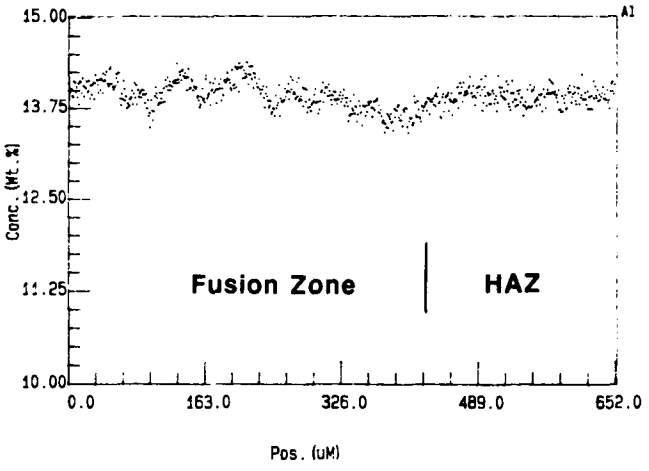

(*c*)

Fig. 13—(*a*) Backscattered electron image of fusion line region in GTA weld in Ti-26Al-11Nb showing position of microprobe profile, (*b*) compositional profile for Ti, Nb, and Al, and (*c*) Al profile shown in greater detail.

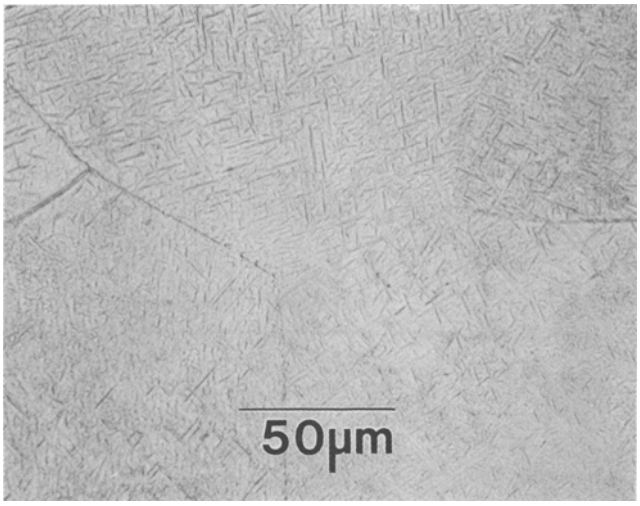

Fig. 14—Optical micrograph of GTA weld fusion zone in Ti-26Al-11Nb.

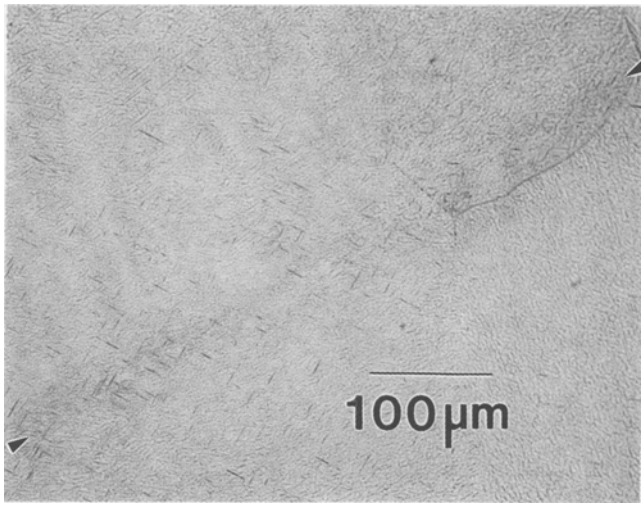

Fig. 15—Optical micrograph of fusion line region in Ti-26Al-11Nb GTA weld. Arrows denote position of fusion line. Note acicular structure is continuous across the fusion line.

Fig. 16—TEM micrograph of fusion zone microstructure in GTA weld metal. Intragranular acicular α_2 laths and grain boundary equiaxed α_2 are both present.

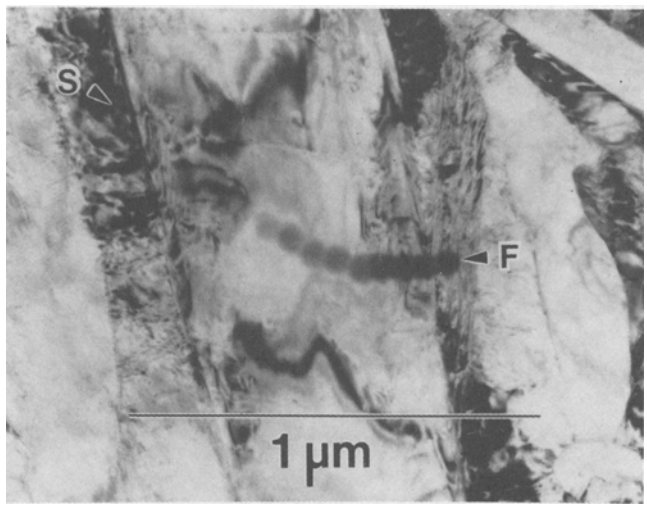

(*a*)

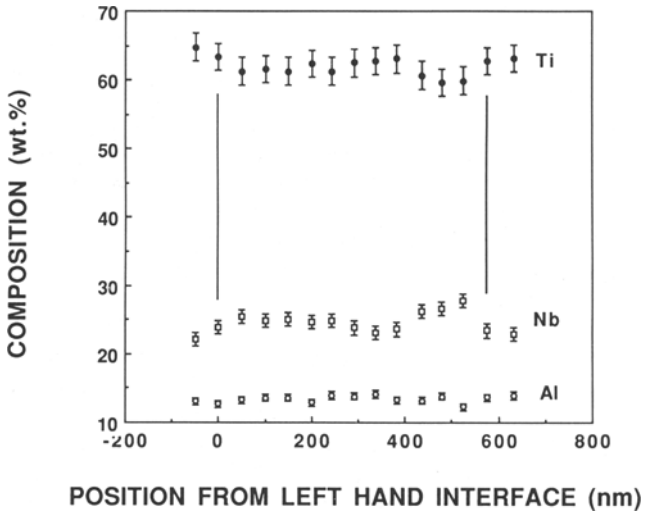

(*b*)

Fig. 17—(*a*) TEM micrograph of acicular lath in GTA weld metal showing location of AEM profile. "S" indicates the start position of the trace and "F" the finish position. Contamination spots can be seen near the end of the trace. (*b*) Compositional profile (vertical lines indicate position of lath boundaries).

is shown in Figures 17(a) and (b). Figure 17(a) shows the position of the contamination spots from the analysis. Within the experimental scatter, no compositional variation within the α_2 lath can be inferred.

Mascorella[7] reported that the ductility of as-GTA-welded samples was poor. He observed longitudinal bend ductilities of generally less than 1 pct (total elastic + plastic strain). An average Knoop hardness (500 gm load) of ≈460 was observed in the fusion zone of the GTA welds. The unaffected $\alpha_2 + \beta$ base metal could support bending strains of 3.5 to 4.5 pct and had an average Knoop hardness of ≈220.

2. *Pulsed Nd:YAG laser welds*

The structure observed in the pulsed Nd:YAG laser welds was substantially different from the GTA welds.

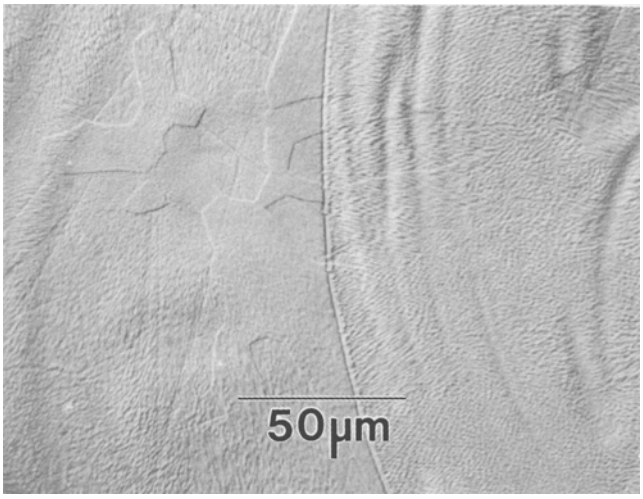

Fig. 18—Optical micrograph of pulsed Nd:YAG laser weld fusion zone in Ti-26Al-11Nb.

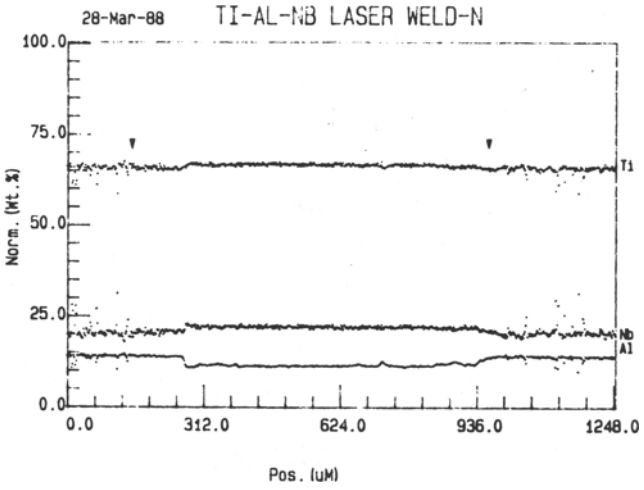

Fig. 20—Electron microprobe profile obtained across the fusion zone in a pulsed Nd:YAG laser weld of Ti-26Al-11Nb. Arrows indicate position of fusion line.

The fusion zone microstructure (Figure 18) was essentially featureless except for the very fine (<1 μm) cellular structure which is likely a remnant of the solidification process. Elemental segregation on the dendritic scale could not be resolved with electron microprobe techniques due to spatial resolution limitations. In contrast, macrosegregation was observed to occur corresponding to the convection pattern observed in the weld metal. Figure 19 is a backscattered electron image of the laser weld showing variations in contrast consistent with the convection pattern developed in the fusion zone. Figure 20 shows an electron microprobe profile taken across the weld (2-μm increments) along the path shown in Figure 19. Aluminum depletion is observed in the bulk of the fusion zone. Local high Al concentrations correspond to dark-appearing regions in Figure 19 (arrows).

Figure 21(a) is a TEM micrograph taken from the fusion zone of the laser weld. An equiaxed grain structure having a relatively low dislocation density is observed.

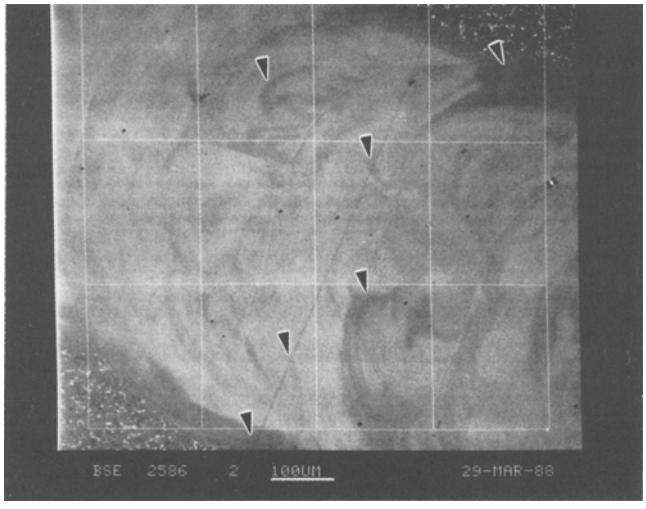

Fig. 19—Backscattered electron image of the fusion zone in a pulsed Nd:YAG laser weld showing convection pattern developed during weld processing. Arrows indicate regions of high Al concentration (Fig. 20).

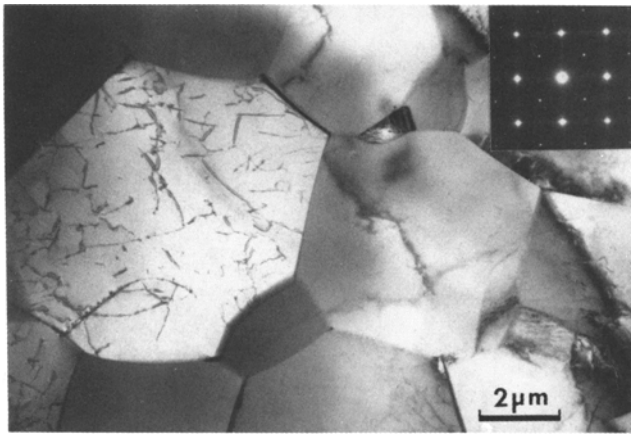

(*a*)

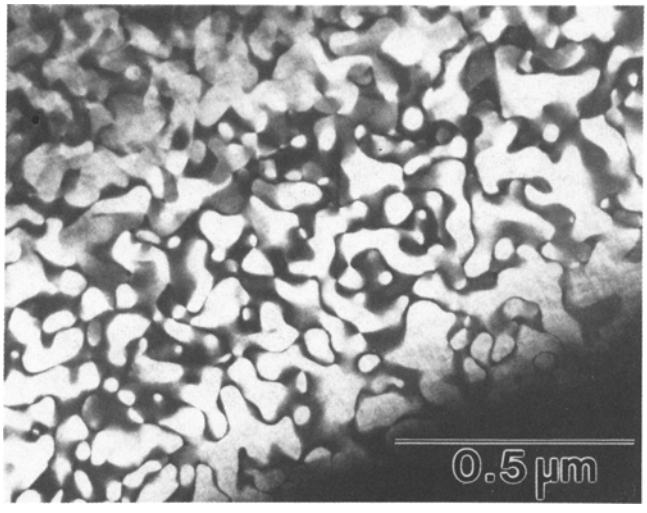

(*b*)

Fig. 21—(*a*) TEM bright-field micrograph of fusion zone microstructure in pulsed Nd:YAG laser weld (diffraction pattern shows [100] β_2 zone. (*b*) TEM dark-field micrograph from β_2 superlattice reflection showing antiphase domain boundary structure in the same laser weld.

Electron diffraction patterns from these grains were consistent with an ordered bcc crystal structure (B2, CsCl structure), hereafter called β_2. Figure 21(b) is a dark-field TEM micrograph taken from a β_2 superlattice reflection showing antiphase domain boundaries resulting from the ordering reaction. In addition, precipitation of a minor constituent having diffraction patterns consistent with α_2 was found occasionally along grain boundaries and on dislocation structures, as shown in the dark-field TEM image of Figure 22.

No evidence of hot cracking was observed in the fusion zones or HAZ's of either the restrained butt-welded sample or any of the other laser welded samples, suggesting a high degree of hot tearing resistance. No hot cracks were observed in any of the GTA bead-on-plate welds. It has been reported previously[8] that as-welded pulsed Nd:YAG laser welds could support bend ductilities similar to that of unaffected $\alpha_2 + \beta$ base metal (3.5 to 4.5 pct, total elastic + plastic). Knoop hardness values (500-gm load) in the fusion zone of these laser welds averaged ≈320.

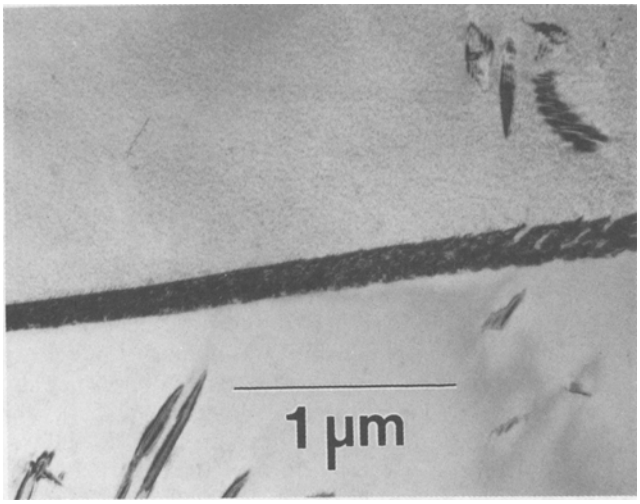

(*a*)

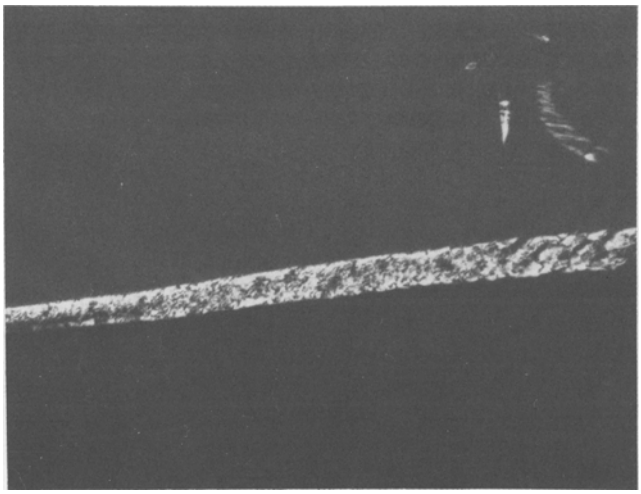

(*b*)

Fig. 22—TEM (*a*) bright-field and (*b*) dark-field images of second phase (α_2) occurring along certain grain boundaries and on dislocations in pulsed Nd:YAG laser weld in Ti-26Al-11Nb.

IV. DISCUSSION

The Discussion is organized into sections which deal with weld solidification and then solid-state transformation behavior. These topics are covered in some detail to provide the necessary insight required to develop an understanding of the expected response of this alloy to fusion welding. Difficulties anticipated as the result of fusion weld processing and requirements for the development of particular microstructures in weld metal are then discussed.

A. *Solidification Behavior*

A ternary phase diagram indicating the tie lines existing in the solidus-liquidus temperature range was not found in the literature. The phase equilibrium information which does exist[13,14] for alloys in this general composition range indicates that β titanium is the stable equilibrium phase just below the solidus.

Solidification of the GTA welds occurred by the epitaxial growth of cells or dendrites on the existing β grains in the HAZ. As seen in Figure 13, the periodic modulation in composition occurs over a spatial range of ≈50 μm. The distribution of the solute atoms, Nb and Al, are in opposite senses. That is, regions of high Nb concentration are regions of low Al concentration. From the binary Ti-Nb phase diagram,[15] Nb raises the melting temperature of Ti-Nb alloys, resulting in a solidification distribution coefficient, k, greater than unity. This implies that the dendrite cores of these alloys will be enriched in Nb and the interdendritic regions will be Nb-lean. Conversely, Al lowers the melting temperature of Ti-Al binary alloys,[16] resulting in a value of k for Al less than unity. This implies that the dendrite cores will be depleted in Al and the interdendritic regions will be Al-rich. If the behavior of Al and Nb in binary Ti alloys can be extrapolated to the ternary alloys, a solidification segregation scenario would develop with Nb-enriched dendrite cores and Al-rich interdendritic regions, as is observed. The distribution of Ti would depend upon which element partitioned more extensively.

The observed room-temperature segregation pattern would also depend upon homogenization of the cellular dendrites both during and subsequent to solidification. Available diffusivity data[17,18] on binary Ti alloys suggest that the rate of homogenization of Al should be greater than that of Nb by approximately an order of magnitude. As seen in Figure 13, Al compositional gradients are much more shallow than those of Ti. Qualitatively then, the observed pattern of alloying element distribution in the GTA weld metal is consistent with the behavior expected of the binary alloys. Without specific values for the distribution coefficients and diffusivities, a more quantitative description of the observed segregation pattern is not possible.

The pulsed Nd:YAG laser welds also solidified in a cellular mode. The cell size is on the order of 1 μm. As primary cell spacing has an approximately inverse square root dependence on the solidification rate,[19] the pulsed

Nd:YAG laser welds solidify 2 to 3 orders of magnitude more rapidly than the GTA welds. The elemental distribution on the cell scale could not be determined by electron microprobe techniques, but macrosegregation was observed, as shown in Figures 19 and 20. This macrosegregation is not related to chemical inhomogeneities in the as-processed sheet. Rather, evaporation of volatile alloying elements during high-energy density-pulsed Nd:YAG laser processing causes this phenomenon. Similar effects have been observed in Mg-bearing aluminum alloys by Cieslak and Fuerschbach.[20] In the case of Ti aluminide, the evaporating component is Al. Corrected for ideal solution activity, Al has the highest vapor pressure of the three components. As shown in Figure 20, Al depletion occurs within the bulk of the fusion zone, but areas near the fusion line are not depleted.

As described previously,[20] the evaporation of volatile alloying elements results in measurable depletion only in areas experiencing enough convection to continue replenishing the surface with these elements. The convection pattern within the fusion zone of a weld is clearly alloy specific.[21] In the case of pulsed Nd:YAG laser welds in Mg-bearing Al alloys,[20] convection loops develop between the fusion line and approximately the 3/4 radius position in a single-pulse weld. Magnesium depletion occurs at this position. In the present case, a stagnant zone develops at the fusion line. Figure 23 shows this dark-appearing zone (lower average atomic number concentration) just within the fusion line. Aluminum concentration in this region is the nominal alloy concentration. It is also likely that Al volatilization will occur to some extent in other high-energy density welding processes, such as electron beam welding, and in processes involving a high surface-to-volume ratio liquid phase, such as thermal (plasma) spraying.

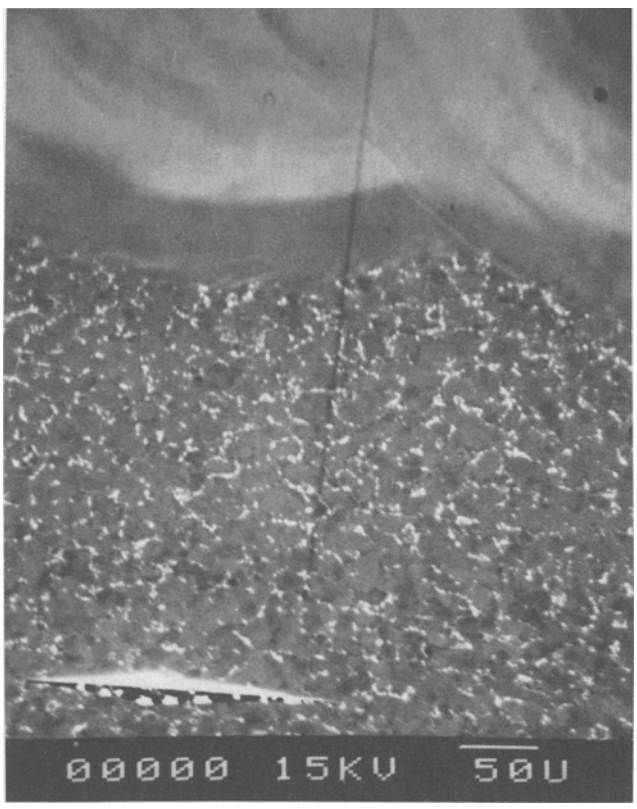

Fig. 23—Backscattered electron image of fusion line region in pulsed Nd:YAG laser weld in Ti-26Al-11Nb. Note dark contrast (low average atomic number concentration, *i.e.*, high Al) region of melted material inside the fusion line.

B. *Solid-State Transformation Structures*

1. *Arc welds and 60 °C/s structures*

The microstructures of the arc welds and the 60 °C/s continuous cooled sample were essentially identical (except for the solidification segregation observed in the arc welds) and will be discussed together (there were no microstructural features in the GTA welds that could be uniquely associated with the remnant solidification segregation pattern). Both had microstructures composed almost entirely of acicular α_2 laths. Occasionally, an equiaxed α_2 structure was also observed at grain boundaries. No β phase was observed anywhere in these microstructures, nor were there any regions of high Nb concentration.

Figure 8 shows the cooling curve obtained during Gleeble testing of the 60 °C/s sample. The transformation temperature is ≈893 °C. The transformation occurs very rapidly, on the order of one second. The β-free acicular microstructure (in contrast to the $\alpha_2 + \beta$ Widmanstätten structure observed at the slowest cooling rate, 0.1 °C/s, Figures 9 through 12) suggests that this transformation occurs in a displacive manner. This transformation mechanism is further supported by the observation of no discernible composition gradients across the acicular laths (Figure 17(*b*)). Displacive transformations are not uncommon in Ti alloys and have been reported in Nb-alloyed (5 at. pct) Ti_3Al by Williams[22] and Sastry and Lipsitt.[23] The transformation temperature may appear high for an 11 at. pct Nb alloy, but Al raises the martensite transformation temperature in Ti alloys. Regression analysis was performed on the M_s data of Jepson *et al.*,[24] the results of which are given in Table III. In the absence of interactive effects, which indeed are likely, an M_s temperature of approximately 805 °C would be expected from a 26 at. pct Al, 11 at. pct Nb alloy. More recently, Morinaga *et al.*[25] have attempted to predict the transformation temperatures in Ti alloys from correlations with first principles electronic structure calculations. For a 26 at. pct Al, 11 at. pct Nb alloy, an M_s temperature >800 °C would be predicted from their calculations.

Previous studies of displacive transformations in Ti alloys almost universally considered transformation from a high-temperature disordered β phase to a lower temperature disordered α' (hexagonal) or disordered α'' (orthorhombic) structure. In the present case, the crystal structure observed in the acicular laths is ordered hexagonal, DO_{19}. It is clear that a displacive transformation

Table III. M_s Relationships*

$M_s^{\text{Ti-Al}}$ [°C] = 880 + 9 (at. pct Al)
$M_s^{\text{Ti-Nb}}$ [°C] = 880 − 9.2 (at. pct Nb) − 1.9 (at. pct Nb)^2

*From regression analysis performed on data of Jepson *et al.*[24]

alone cannot produce an ordered daughter phase from a disordered parent. The observed microstructure could then be evolved by either of the following two mechanisms. In the first case, disordered β could shear to α' with the subsequent ordering reaction, $\alpha' \Rightarrow \alpha_2'$. The second case would have β ordering to the B2 crystal structure with a subsequent shear to α_2, or rather α_2', to be consistent with the existing terminology. The $\beta \Rightarrow \alpha'$ transformation is common, whereas the $\beta_2 \Rightarrow \alpha_2'$ shear transformation has not been reported and may not be structurally or thermodynamically possible.

In either case, a transformation involving a combination of shear and ordering would result in the final transformed microstructure having ordered domains. The absence of ordered domains would suggest that the transformation occurred by a nucleation-and-growth mechanism, $\beta \Rightarrow \alpha_2$. Figures 24(a) through (c) show a sequence of bright-field/dark-field TEM images of an acicular lath in the GTA weld. Imaging the α_2 superlattice reflection, $11\bar{2}0$, reveals antiphase domain boundaries. We did not observe these domains crossing lath boundaries.

Sastry and Lipsitt[23] observed a displacive transformation ($\beta \Rightarrow \alpha'$) resulting in an acicular α' structure in the system Ti-26.6Al-4.94Nb at. pct subsequent to water quenching from 1250 °C. They reported no ordered domains in the acicular α' but suggest that fine domains, below the resolving capability of their analysis, could be present. Domain structures were observed in their alloy after heat treatment in the α_2 region (≈900 °C). Water-quenched samples of the binary alloy, Ti-26.8Al at. pct, did contain ordered domains in a massive martensitic structure, suggesting that (1) the ordering reaction in this binary alloy was very rapid in comparison to the Nb-alloyed material and (2) that the transformation sequence $\beta \Rightarrow \alpha' \Rightarrow \alpha_2'$ was reasonable in this alloy type. No continuous cooling experiments in the cooling rate regime associated with arc welding were reported by these authors, so direct comparison with the present work is not possible.

The mechanism of displacive transformation in titanium alloys is somewhat more involved than similar transformations in iron alloys. Jepson *et al.*[24] showed that the transformation start temperature was itself a function of cooling rate for Ti-Nb and Ti-Al alloys, with lower M_s temperatures at higher rates of cooling, implying that the displacive transformation is not truly athermal in these cases. Mascorella[7] observed the same effect during the development of a continuous cooling transformation diagram for Ti-26Al-11Nb. That is, an acicular α_2 structure was developed over a cooling rate range of 1 °C to 150 °C/s, with the transformation start temperature falling with increased cooling rate. At the fastest cooling rate (150 °C/s), the transformation temperature was ≈800 °C. Transmission electron microscopy was not used to characterize the microstructures observed in that study.

The collected data from this study and previous investigations suggest that the development of the acicular α_2 structure in Ti-26Al-11Nb involves a combination of displacive and ordering mechanisms.

The observation of an equiaxed grain boundary α_2 constituent in the presence of a martensitic α_2 microstructure is not unique to this study. Williams[22] showed

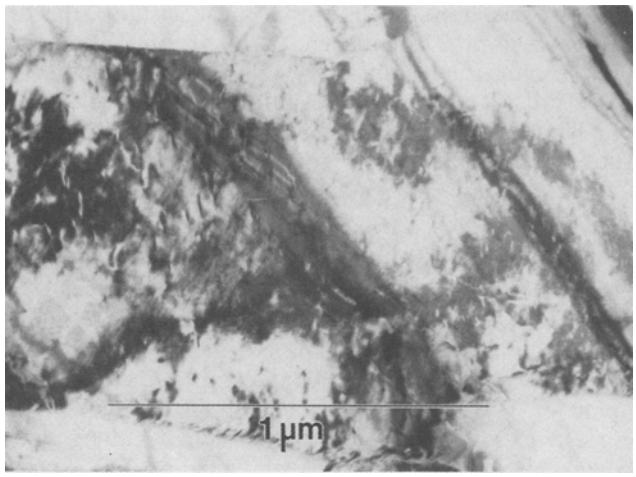

(*a*)

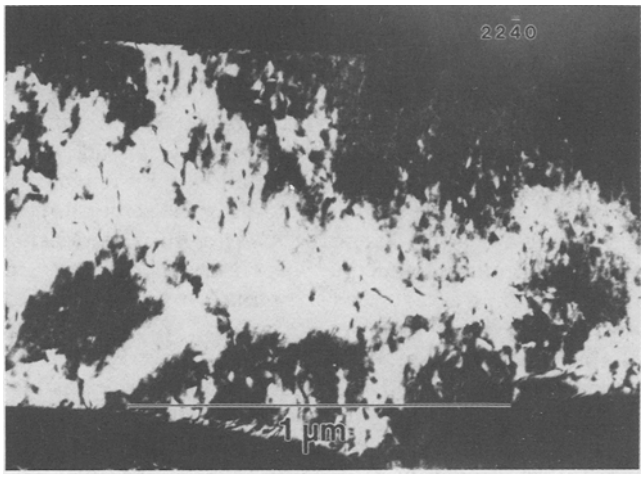

(*b*)

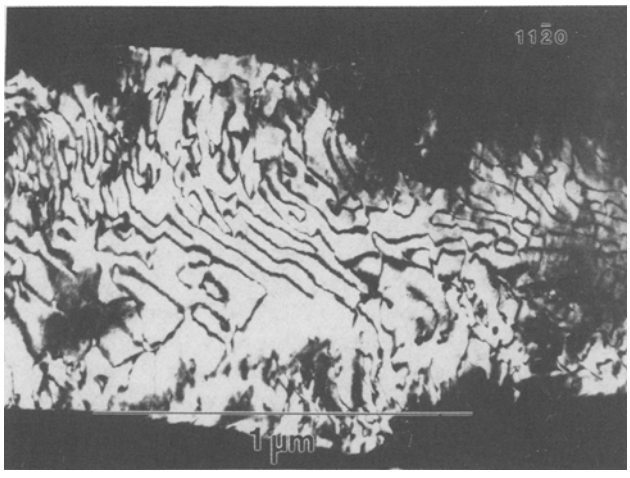

(*c*)

Fig. 24—TEM images of α_2 lath in GTA weld metal fusion zone: (*a*) bright-field and (*b*) dark-field image from $22\bar{4}0$ of α_2, and (*c*) dark-field image from superlattice reflection $11\bar{2}0$.

previously that an autorecrystallization phenomenon can occur in Ti-25Al-5Nb at. pct (martensitic microstructure) as a result of thermal processing subsequent to water quenching. An equiaxed α_2 grain boundary

structure was developed. In the present study, the decomposition of β to the acicular α_2 structure occurs at a high enough temperature ($\approx$900 °C) that initiation of a recrystallization event, resulting in the development of a limited equiaxed grain boundary α_2 constituent, during subsequent cooling to room temperature, is not unreasonable.

2. *Pulsed Nd:YAG laser welds*

The microstructure observed in the fusion zone of the pulsed Nd:YAG laser welds was featureless on the optical microscopy scale except for remnants of the cellular solidification pattern. Transmission electron microscopy examination revealed a structure comprised of equiaxed grains of β_2 with precipitates having diffraction patterns consistent with α_2 occurring occasionally along grain boundaries and on dislocations within the β_2. The ω phase was not unequivocally identified during the diffraction analysis.[8]

Retention of β phase and ordering of high-temperature β during rapid cooling below the β solvus has been observed previously.[8–10,24] In a study examining binary Ti alloys, Jepson *et al.*[24] observed β retention (by X-ray diffraction analysis) in a Ti-17.5Nb at. pct alloy during rapid cooling ($>10^4$ °C/s). No mention was made of an ordered β constituent (optical metallography revealed a featureless, equiaxed grain structure). In the same alloy,[24] at cooling rates less than 10^4 °C/s, a fully martensitic (α'', orthorhombic) structure was observed. An equiaxed ordered β grain structure was observed in water-quenched Ti-28Al-12Nb at. pct by Strychor, Williams, and Soffa.[9,10] In addition, diffuse ω was observed during the diffraction analysis. This phase became more distinct during subsequent aging treatments. Finally, Mascorella[7] observed a relatively low hardness, featureless microstructure in samples of Ti-26Al-11Nb both water quenched from 1200 °C and in certain electron beam welds.

The β ordering reaction temperature for this alloy was not determined in this study. The fine domain structure in the β_2 is consistent with a rapid cooling through the ordering temperature range and a suppression of thermally activated domain growth.[23] The apparent presence of α_2 located on defect sites in this microstructure was not observed by Strychor *et al.*[9] It is most likely that the previous study involved quench rates greater than those experienced in the present investigation. In the work of Strychor *et al.*,[9] 0.75-mm-thick samples were water quenched after solutionizing at 1250 °C. In the present study, cooling of the pulsed Nd:YAG laser weld occurs predominantly by conduction laterally through the 1.7-mm sheet, which likely results in slower cooling rates. In addition, the alloy used by Strychor *et al.*[9] was somewhat more enriched in Nb and Al than that used in this study. As stated above, cooling rates slower than 150 °C/s result in microstructures involving α_2. We did not determine the critical cooling rate required to completely suppress α_2 formation in this alloy, but apparently, it is greater than that achieved during pulsed Nd:YAG laser welding under the conditions of this experiment.

3. *0.1 °C/s structures*

The microstructure observed in the 0.1 °C/s continuously cooled sample was a duplex microstructure of α_2, often referred to as a colony structure, and retained β. This microstructure exhibits the Widmanstätten-type morphology characteristic of a nucleation-and-growth mechanism. Alloying element segregation occurs in the expected sense of a diffusionally controlled phase transformation. That is, Nb, a β stabilizer, partitions to the retained β and Al, an α stabilizer, and Ti partition to the α_2 phase.

Dark-field electron diffraction experiments revealed that ordered domains were not present within the α_2. The lack of ordered domains in the α_2 further suggests a nucleation-and-growth transformation mechanism of α_2 from β. Although the lack of domains is a necessary condition for the transformation $\beta \Rightarrow \alpha_2$, it is not a completely sufficient condition. That is, the transformation from β to α_2 could occur *via* an intermediate transformation to disordered α. α would then order to α_2, leaving behind a domain structure. At this very slow cooling rate, thermally activated domain growth could result in each α_2 colony being a single ordered domain. Antiphase domain boundaries would not then be observed during the TEM analysis. Support that this scenario is not occuring comes from the available phase diagram data,[9,13,14] which identifies no regions of disordered α stability in the composition/temperature range relevant to this study. (The appearance of α' as a nonequilibrium transition structure at rapid cooling rates, as proposed above, is not inconsistent with the previously proposed phase equilibrium data.[9,13,14]) That is, as the equilibrium cooling rate is approached, the presence of disordered α could not be inferred from the available phase stability data. Independent of the actual transformation sequence which results in the observed microstructure, though, it is clear that at this cooling rate, diffusionally controlled mechanisms are responsible for the microstructural evolution. The presence of a chemically modified (Nb-rich, Ti and Al-lean) retained β unequivocally shows that diffusive processes were occuring. The evolution of a chemically segregated, two-phase microstructure at this slow cooling rate also gives further support to the proposed displacive transformation sequence in both the arc-welded and 60 °C/s cooling rate Gleeble samples discussed above.

4. *Summary of continuous cooling transformation behavior*

From the results and discussion presented above and the collected data of other relevant studies,[1–10,22–24] a schematic continuous cooling transformation diagram for Ti-26Al-11Nb can be developed, as shown in Figure 25. It can be seen that three transformation paths are possible in Ti-26Al-11Nb. At very rapid cooling rates such as those experienced in water quenching or pulsed Nd:YAG laser welding, the $\beta \Rightarrow \alpha_2$ transformation is essentially suppressed and β orders to the B2 crystal structure. In the cooling rate range of normal industrial processing (hot working, welding, casting), $\approx$1 °C to 100 °C/s, an acicular α_2 microstructure is formed. The experimental data strongly suggest that this transformation involves a martensitic component. That the transformation temperature is a function of cooling rate indicates a nonathermal nature of this shear transformation. At very slow cooling rates, 0.1 °C/s, characteristic of furnace cooling, a diffusionally produced

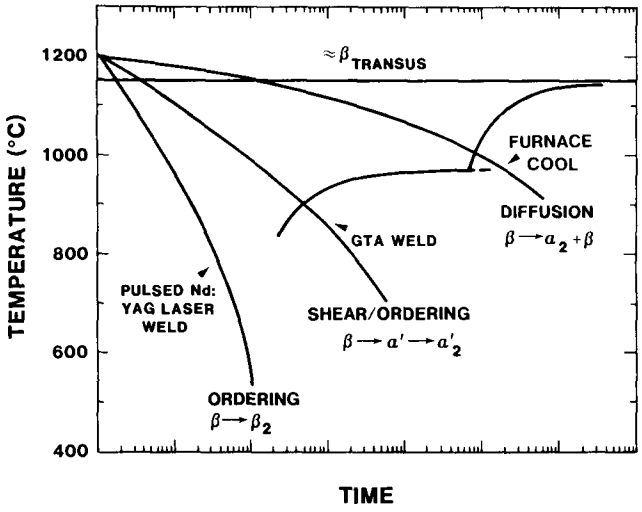

Fig. 25—Schematic continuous cooling transformation diagram for Ti-26Al-11Nb. Approximate cooling rates for various industrial processes are indicated.

transformation structure of colony α_2 and retained β is observed. With the exception of the β ordering reaction, this diagram is consistent with those developed by Jepson *et al.*[24] for heavily alloyed Ti-Nb binary alloys.

C. *Applications to Fusion Welding*

All fusion welding operations necessarily produce a thermal excursion which results in the fusion zone and at least part of the HAZ entering into the temperature regime of single-phase β stability. The room-temperature microstructure and resultant mechanical properties then become a function of the cooling rate from the β solvus.

From experiences obtained during welding of Ti-26Al-11Nb in this study, it can be concluded that solidification cracking would not be a problem anticipated during commercial fusion welding operations using the processes employed here. Although the bead-on-plate GTA welds are not highly restrained, an unweldable alloy would be expected to contain readily observable defects. An absence of cracking in the restrained, pulsed Nd:YAG laser butt welds indicates good resistance to hot cracking by this rapid solidification process.

Generally, poor engineering ductility in arc-welded Ti-26Al-11Nb can be attributed to the development of the hard, acicular, dislocated α_2 microstructure. As shown earlier by Mascorella,[7] this acicular structure and its attendant low ductility persists over the cooling rate range of 1 °C to 150 °C/s. Potentially more disturbing is the reality that when the transformation to α_2 occurs, a more close-packed crystal structure is formed, resulting in a bulk shrinkage of the fusion zone and parts of the HAZ.[7] In highly restrained weld joints, the potential for catastrophic failure of welded hardware exists as the joints cool and transform into a low ductility microstructure.

Williams[22] has shown that this microstructure in Ti-25Al-5Nb at. pct, identified as a martensitic product, is thermally unstable. Exposure below the β solvus resulted in a self-induced autorecrystallization that degraded mechanical properties. Williams[22] suggests that the development of nucleation-and-growth-type structures would be preferred from the standpoint of microstructural stability.

In considering the transformation products observed in the present study and those observed earlier,[7] it is clear that very slow cooling rates, <1 °C/s, are required to develop a complete nucleation-and-growth-derived microstructure on cooling from the β solvus. In the present study, a cooling rate of 0.1 °C/s produces such a microstructure. To obtain this cooling rate and microstructure in the fusion zone of arc welds requires that the cooling rate be suppressed in some manner. For full penetration welds in thin sheet product, the heat flow behavior is approximately two-dimensional (2-D) in nature. An approximation of the cooling rate, $\partial T/\partial t$, at the centerline of such a weld can be obtained from the following analytical expression:[26]

$$\partial T/\partial t = 2\pi k\rho c(z/\eta H)^2(T_c - T_0)^3$$

where k is the thermal conductivity, ρ is the density, c is the heat capacity, z is the sheet thickness, H is the linear energy input, T_c is the temperature at which the cooling rate is determined, T_0 is the sheet preheat temperature, and η is the arc efficiency, all in appropriate units. From this expression, it can easily be seen that the most effective manner of decreasing the cooling rate is by preheating the sheet (increasing T_0), as this variable has a cube dependence. The specific thermophysical properties for this alloy are not known but can be calculated as a group from other data. Mascorella[7] observed that the hardness of Gleeble samples, continuously cooled from the β solvus at a rate of 60 °C/s, was identical to that observed in the fusion zone of full penetration GTA welds (2-D heat flow) made using the welding parameters given above (90 Amps, 10.5 Volts, 4.2 mm/s travel speed). For a cooling rate of 60 °C/s, using an arc efficiency of 0.8,[27] a transformation temperature, T_c, of 900 °C and a preheat of 20 °C (room temperature), a value for the collected group of premultiplying constants of 9.87×10^{-4} J^2([°C]^2[s][mm]^4)$^{-1}$ was obtained. To produce a cooling rate of 0.1 °C/s in the same sheet material would now require a preheat of ≈795 °C.

It is clear that fusion weld processing of this alloy under this preheating requirement would not be desirable. The slow cooling rate required to produce an equilibrium-type microstructure in this alloy results from an inability to nucleate the low-temperature α_2 from the β matrix. The nucleation problem could be caused by the low diffusivities expected in this alloy (the chemical diffusivity of Nb in Ti decreases with increasing Nb concentration).[17,18] Another contributing factor may be the difficulty of nucleating an ordered (α_2) rather than a disordered phase. Traditionally, to cause nucleation-and growth-type transformations to occur at faster cooling rates requires either making compositional modifications to increase diffusion rates or reducing grain size to produce more heterogeneous nucleation sites. Grain size modifications are not likely to generate much benefit, as the nature of the solidification process in arc welding produces relatively large grains, especially in the fusion zone and in the near HAZ. Compositional modifications may prove somewhat more effective. At the present time, though, no systematic investigation of alloying element

effects on the continuous cooling transformation diagrams for alloys of this general type has been reported in the open literature.

Pulsed Nd:YAG laser welding appears to offer an intriguing method of producing a fusion weld with reasonable ductility approximately equal to the base metal. As shown earlier by Strychor, Williams, and Soffa,[9,10] this microstructure is also metastable relative to ω, and ultimately, α_2 formation. But by suppressing the transformation to an acicular α_2 structure, the possibility exists of developing postweld heat treatment cycles which can tailor the microstructure in a manner which results in improved mechanical properties. Because welding with high-energy density processes (laser and electron beams) localizes the energy source in such a small area on the workpiece, stringent machining tolerances will be required to affect acceptable joints.

It can be anticipated that this alloy will be difficult to incorporate into GTA welded designs because of the limited ductility of welded product. Greater possibilities exist for high solidification rate (laser, electron beam) fusion welding, but these will necessarily require the development of postweld heat treatments to both stabilize microstructure and produce weld joints with mechanical properties having engineering utility.

V. CONCLUSIONS

The phase transformations resulting from fusion weld and solid-state processing of Nb-alloyed titanium aluminide (Ti-26Al-11Nb at. pct) have been characterized. The very rapid cooling rates characteristic of pulsed Ng:YAG laser welding resulted in ordering of the high-temperature β phase in lieu of transformation to the lower temperature α_2 phase. Gas-tungsten-arc weld processing (cooling rate $\approx$60 °C/s) resulted in the formation of a microstructure completely transformed to an acicular α_2 phase likely arising from a combination of displacive and ordering mechanisms. As reported previously, the pulsed Nd:YAG laser welds have better ductility than the GTA welds. An equilibrium-type $\alpha_2 + \beta$ microstructure is achieved in this alloy at a cooling rate from the β solvus of 0.1 °C/s. Calculations show that this cooling rate could be achieved in GTA welds in 1.7-mm-thick sheet when preheats of $\approx$795 °C are employed. Possibilities for microstructural tailoring exist with the pulsed Nd:YAG laser welds to optimize mechanical properties. Solidification cracking should not be anticipated during the fusion welding of this alloy.

ACKNOWLEDGMENTS

The authors would like to acknowledge Tom Lienert and Tim Mascorella for performing the welding experiments, Mark MacAllaster for the metallographic assistance, and Ellen Semarge for performing the electron microprobe experiments. We thank General Electric Company, Evandale, OH, for providing the material and chemical analysis for this investigation. We thank Al Romig and Marty Carr for assistance with the reduction of AEM/EDS data. Discussions with Jim Williams, Doug Polonis, Pat Martin, and Mike Kaufman are gratefully acknowledged. We also thank John Stephens and Roy Bourcier for reviewing the manuscript. This work was performed at Sandia National Laboratories, supported by the United States Department of Energy under Contract No. DE-AC04-76DP00789.

REFERENCES

1. H.A. Lipsitt: *High Temperature Ordered Intermetallic Alloys*, MRS, Symp. Proc., C.C. Koch, C.T. Liu, and N.S. Stoloff, eds., 1984, pp. 351-64.
2. F. LeMaitre: *Mém. Sci. Rev. Métall.*, 1970, pp. 563-74.
3. K.C. Wu: *Weld. J.*, 1981, pp. 219s-226s.
4. F.D. Mullins and D.W. Becker: *Weld. J.*, 1980, pp. 177s-182s.
5. W.A. Baeslack III and C.M. Banas: *Weld. J.*, 1981, pp. 121s-130s.
6. W.A. Baeslack III and F.D. Mullins: *Metall. Trans. A*, 1984, pp. 1948-52.
7. T.J. Mascorella: M.S. Thesis, The Ohio State University, Columbus, OH, 1987.
8. W.A. Baeslack III, M.J. Cieslak, and T.J. Headley: *Scripta Metall.*, 1988, pp. 1155-60.
9. R. Strychor, J.C. Williams, and W.A. Soffa: *Metall. Trans. A*, 1988, pp. 225-34.
10. R. Strychor and J.C. Williams: *Solid ⇒ Solid Phase Transformations*, Hubert I. Aaronson, David E. Laughlin, Robert F. Sekerka, and C. Marvin Wayman, eds., TMS, Warrendale, PA, 1982, pp. 249-53.
11. *Gleeble 1500*, Duffers Scientific, Inc., Troy, NY.
12. W.F. Chambers: Sandia Report SAND85-2037, Albuquerque, NM, 1985.
13. T.T. Nartova and G.G. Sopochkin: *Russ. Metall. (Metally)*, 1970, p. 138.
14. O.N. Andreyev: *Russ. Metall. (Metally)*, 1970, p. 127.
15. *Metals Handbook*, 8th ed., ASM INTERNATIONAL, Metals Park, OH, 1973, vol. 8, p. 284.
16. *Metals Handbook*, 8th ed., ASM INTERNATIONAL, Metals Park, OH, 1973, vol. 8, p. 264.
17. *Smithells Metals Reference Book*, 6th ed., E.A. Brandes, ed., Butterworth's, London, 1983, pp. **13**-56 and **13**-71.
18. D.L. Moffat and U.R. Kattner: *Metall. Trans. A*, 1988, pp. 2389-97.
19. M.C. Flemings: *Solidification Processing*, McGraw-Hill, New York, NY, 1974, p. 148.
20. M.J. Cieslak and P.W. Fuerschbach: *Metall. Trans. B*, 1988, pp. 319-29.
21. C.R. Heiple and J.R. Roper: *Trends in Welding Research in the United States*, S.A. David, ed., ASM INTERNATIONAL, Metals Park, OH, 1982, pp. 489-515.
22. J.C. Williams: *Titanium and Titanium Alloys*, J.C. Williams and A.F. Belov, eds., Plenum Press, Oxford, 1982, pp. 1477-98.
23. S.M.L. Sastry and H.A. Lipsitt: *Metall. Trans. A*, 1977, pp. 1543-52.
24. K.S. Jepson, A.R.G. Brown, and J.A. Gray: *The Science, Technology and Application of Titanium*, R.I. Jaffee and N.E. Promisel, eds., Pergamon Press, Oxford, 1966, pp. 677-90.
25. M. Morinaga, N. Yukawa, and H. Adachi: *Tetsu-to-Hagané*, 1986, no. 6, pp. 21-28.
26. D. Rosenthal: *Trans. AIME*, 1946, pp. 849-66.
27. G.A. Knorovsky and P.W. Fuerschbach: *Proc. Int. Conf. on Advances in Welding Science and Technology*, S.A. David, ed., ASM INTERNATIONAL, Metals Park, OH, 1986, pp. 393-400.